

A Novel Technique for Long-term Timing of Redback Millisecond Pulsars

KYLE A. CORCORAN,^{1,*} SCOTT M. RANSOM,² ALEXANDRA C. ROSENTHAL,¹ MEGAN E. DECESAR,^{3,4}
PAULO C. C. FREIRE,⁵ JASON W. T. HESSELS,^{6,7} RYAN S. LYNCH,⁸ PRAJWAL V. PADMANABH,^{9,10} AND
INGRID H. STAIRS¹¹

¹University of Virginia, Department of Astronomy, Charlottesville, VA 22904, USA

²National Radio Astronomy Observatory, Charlottesville, VA 22903, USA

³George Mason University, Fairfax, VA 22030, USA

⁴Resident at the U.S. Naval Research Laboratory, Washington, DC 20375, USA

⁵Max-Planck-Institut für Radioastronomie, Auf dem Hügel 69, D-53121 Bonn, Germany

⁶Anton Pannekoek Institute for Astronomy, University of Amsterdam, Science Park 904, 1098 XH Amsterdam, The Netherlands

⁷ASTRON, Netherlands Institute for Radio Astronomy, Oude Hoogeveensedijk 4, 7991 PD Dwingeloo, The Netherlands

⁸Green Bank Observatory, P.O. Box 2, Green Bank, WV 24494, USA

⁹Max Planck Institute for Gravitational Physics (Albert Einstein Institute), D-30167 Hannover, Germany

¹⁰Leibniz Universität Hannover, D-30167 Hannover, Germany

¹¹Department of Physics and Astronomy, University of British Columbia, 6224 Agricultural Road, Vancouver, BC V6T 1Z1 Canada

ABSTRACT

We present timing solutions spanning nearly two decades for five redback (RB) systems found in globular clusters (GC), created using a novel technique that effectively “isolates” the pulsar. By accurately measuring the time of passage through periastron (T_0) at points over the timing baseline, we use a piecewise-continuous, binary model to get local solutions of the orbital variations that we pair with long-term orbital information to remove the orbital timing delays. The isolated pulse times of arrival can then be fit to describe the spin behavior of the millisecond pulsar (MSP). The results of our timing analyses via this method are consistent with those of conventional timing methods for binaries in GCs as demonstrated by analyses of NGC 6440D. We also investigate the observed orbital phase variations for these systems. Quasi-periodic oscillations in Terzan 5P’s orbit may be the result of changes to the gravitational-quadruple moment of the companion as prescribed by the Applegate model. We find a striking correlation between the standard deviation of the phase variations as a fraction of a system’s orbit ($\sigma_{\Delta T_0}$) and the MSP’s spin frequency, as well as a potential correlation between $\sigma_{\Delta T_0}$ and the binary’s projected semi-major axis. While long-term RB timing is fraught with large systematics, our work provides a needed alternative for studying systems with significant orbital variations, especially when high-cadence monitoring observations are unavailable.

Keywords: Millisecond Pulsars (1062) — Spider Pulsars, Globular star clusters (656)

1. INTRODUCTION

Millisecond pulsars (MSPs) with binary companions are an interesting class of radio pulsars and unique laboratories for various tests of fundamental physics. These neutron stars have been spun up via accretion of material from a close binary companion (Alpar et al. 1982), and we most commonly observe the resultant system

in a relatively wide orbit with a low-mass, white dwarf companion (Manchester et al. 2005; Tauris & van den Heuvel 2006, for a survey of this topic see Tauris & van den Heuvel 2023).

1.1. “Redback” pulsars

A portion of systems with other companion types can evolve to much more compact orbits ($P_b < 1$ day), and one such sub-class is called Redbacks (RBs). These MSPs are members of the “spider” pulsar family and have H-rich, non-degenerate companions that have masses typically between $0.1M_\odot < M_c < 0.9M_\odot$ (Roberts 2013; Strader et al. 2019). RBs typically have

Corresponding author: Kyle A. Corcoran

kcorcoran@cp.i.com

* Computational Physics, Inc.

orbital periods of only a few hours, and their neutron star masses are generally found to exceed $1.4 M_{\odot}$ (Strader et al. 2019). Additionally, RBs are exceptional producers of multi-wavelength emission, producing features such as radio pulsations, γ -ray pulsations (Deneva et al. 2021; Thongmeearkom et al. 2024), and optical light-curve variations (Bellm et al. 2016; Yap et al. 2023).

Due to their compact nature, binary interactions play a large role in the evolution and observed properties of RBs. The intense pulsar wind ablates material from the companion, creating circumbinary, ionized material. This material can cause radio eclipses – most likely caused by synchrotron absorption (Polzin et al. 2018) – that can shroud radio pulsations for significant portions of the orbit (Nice et al. 1990) around superior conjunction. These eclipses can be highly irregular, though, and dependencies on observing frequency can further impact the duration and appearance of any one eclipse (e.g., Nice et al. 1990; You et al. 2018). Additional eclipse-like events due to material at other orbital phases can also mask pulsations (e.g., Bilous et al. 2019), and the long-term behavior of the binary orbit in RBs has been observed to wander drastically (Prager 2017; Clark et al. 2021; Thongmeearkom et al. 2024). These factors limit the accuracy of binary models to describe the system over time.

Timing studies of MSPs in binaries given sufficient baselines can yield insights into interesting physics in areas such as general relativity (e.g., Kramer et al. 2021, see Freire & Wex 2024 for a review) and the neutron star equation of state (Fonseca et al. 2021); however, the barrage of impediments listed above means that despite their potentially large NS masses, RBs are often excluded from consideration for long-term timing efforts in the radio. Obtaining successive detections – let alone detections over short to long baselines – of the MSP can be difficult, and linking observations together in a way that yields insights into the physical characteristics of these systems is also non-trivial. While the binary interactions in RBs may not make them ideal test beds for probing the most impactful binary physics, accurate measurements of physical properties derived from long-baseline timing still would yield important limits for modeling the companion’s interior and binary evolution modeling. These limits can inform a variety of interesting cases. The majority of published radio-timing solutions for RBs, however, only cover a baseline of a few years (Archibald et al. 2013; Prager 2017; Miraval Zanon et al. 2018; Deneva et al. 2021; Padmanabh et al. 2024; Ghosh et al. 2024). Thongmeearkom et al. (2024) achieved phase connection using γ -ray data from the *Fermi* Large

Area Telescope (LAT), which spans 15 years, but this technique requires that the pulsars are bright in γ rays. Nice et al. (2000) and Ridolfi et al. (2016) presented radio-timing solutions for around a decade of targeted observations of two redback systems in the globular clusters Terzan 5 and 47 Tucanae, B1744–24A (henceforth Ter5A) and PSR J0024–7204W (47 Tuc W). Targeted radio observations or even archival radio data spanning this duration or longer for individual RBs are generally not available, making these long-term studies difficult to conduct.

However, the main obstacle preventing long-term timing studies of RBs is the limitations of the orbital timing models. The BTX model, which is the one currently used to describe the orbital evolution of RBs, use multiple orbital frequency derivatives in a Taylor expansion of the orbital phase with time. Such models are not predictive, however, that is not their main problem: many orbital frequency derivatives are needed in most cases. This implies that outside their range of validity, the higher order derivatives completely dominate the expansion, leading to explosive non-physical predictions for the variation of the orbital period. This leads to very poor predictions for the orbital phase outside the range of data used to derive them, making even the folding procedure unreliable.

1.2. Globular cluster pulsars

Globular clusters (GCs) present an opportunity to provide long-term baselines for RBs by exploiting observations of the cluster aimed at the pulsar population. Per unit of stellar mass, GCs have more than 3 orders of magnitude more X-ray binaries and MSPs than the Galactic disk; this suggests that these systems formed dynamically, which is possible in GCs because of their very large stellar densities (Ransom 2008; Freire 2013). One of the interesting features of the pulsar population in GCs is that, in the densest of them, exchange encounters can happen after the pulsar was recycled, allowing the formation of systems that are unlike any formed in the Galactic disk. This applies to RBs as well: Unlike in the case of the Galactic RBs, some of the RBs in GCs might be the product of pair exchange (where the star that spun up the pulsar is ejected and replaced with a more massive star; Ransom et al. 2005; Prager 2017). In any case, GCs have a disproportionately large number of RBs compared to the Galactic pulsar population.

Given the very large distances of GCs, only a small fraction of their MSPs has been discovered, with the majority remaining undetected due to sensitivity limitations. This means that observations with improved sensitivity allow the discovery of new pulsars; they also

result in improved timing of previously known pulsars. One of the benefits of timing pulsars in GCs is to use pulsars as accelerometers, which allow constraints on GC mass models. This is especially true of GCs that contain a large population of pulsars, like Terzan 5 (Prager et al. 2017) and 47 Tucanae (Freire et al. 2017; Abbate et al. 2018).

Terzan 5 (hereafter Ter5) has the largest known population of pulsars in any GC (49; Padmanabh et al. 2024) with over half being in binaries – four of which are RBs. Ter5A is the first ever RB discovered (Lyne et al. 1990; Nice et al. 1990, 2000) and one of the most compact RBs known; Ter5ad is the record holder for the fastest spinning MSP ($P \sim 1.39$ ms; Hessels et al. 2006); Ter5P is also rapidly spinning ($P \sim 1.72$ ms), has the second largest mass fraction for RBs due to its more massive companion ($M_{c,\min} \sim 0.38 M_{\odot}$) and Ter5ar is the most recently discovered, rapidly rotating ($P \sim 1.95$ ms) RB with a larger mass companion ($M_{c,\min} \sim 0.34 M_{\odot}$) as well (Padmanabh et al. 2024). A smaller population of binary pulsars is found in M28, and it, too, contains RBs – M28I, which is a transitional MSP (switches between a radio pulsar state and a low-mass X-ray binary state; Papitto et al. 2013), and M28H, which is another RB thought to be the product of pair exchange (Pallanca et al. 2010; Bogdanov et al. 2011). NGC 6440, which has the smallest binary population of the three clusters mentioned here, also hosts a RB, NGC 6440D (Freire et al. 2008), that exhibits relatively stable orbital variations (Ransom et al., in prep). These three GCs have been actively monitored for nearly the past 20 years through observations at various frequencies using the Green Bank Telescope (GBT), making them unique sources to test RB timing methods on a longer scale than has previously been possible.

1.3. Structure of this work

In §2 we briefly describe the roughly 20 years of archival data from the GBT. In §3 we present a novel technique for “isolating” the MSP from the orbital effects of the binary companion, allowing us to time the underlying, highly accurate clock. This method effectively overcomes the aforementioned limitations of the BTX model, allowing long-term timing of RBs. In §4 we present our long-term timing analysis of five RBs in GCs – Ter5P, Ter5ad, Ter5ar, M28H, and NGC 6440D, our fully phase-connected timing solutions, the long-term orbital variations that were removed to create them, and pulse profiles (shown in Figure 1) for each system. Apart from NGC 6440D, none of these pulsars had any published timing solutions until now. A separate publication on 34 years of timing of another RB, Ter5A, that

uses the same technique is presented in Rosenthal et al. (2024). We then discuss the results from our technique and how they compare to those of conventional timing methods, the quasi-periodic oscillations seen in Ter5P, and a correlation between orbital variations and spin frequency in §5. Finally, we summarize our work in §6.

2. OBSERVATIONS

We used archival data for each cluster from observations with the GBT spanning roughly 20 years. A majority of our data were taken using S-band (1600-2400 MHz) and L-band (1100-1900 MHz) receivers with ~ 600 -700 MHz of useable bandwidth in each case. Additionally, a smaller fraction of data were taken at 820 MHz. In our data, the GBT Pulsar SPIGOT (Kaplan et al. 2005) backend was used for all observations prior to MJD 55000, the GUPPI (DuPlain et al. 2008) backend was then used for observations up until MJD 58933, and that same day the VEGAS (Prestage et al. 2015) backend was switched onto the GBT¹. The SPIGOT data were taken using incoherent dedispersion, and detailed information about the observations for Ter5, which were obtained in a consistent manner to the observations for M28H and NGC 6440, can be found in Ransom et al. (2005). Prior to MJD 55422, observations using GUPPI (only a few scans for each system) were also obtained with incoherent dedispersion; the remaining GUPPI and VEGAS observations were taken using coherent dedispersion, and detailed information about the observations for Ter5 can be found in Martsen et al. (2022). As with SPIGOT, the GUPPI and VEGAS observations were obtained in a consistent manner to those for M28H and NGC 6440, with the obvious exception of the dispersion measure (DM) where the coherent data are dedispersed.

3. TIMING METHODOLOGY

In the text that follows we introduce the prescription for and our workflow implementation of the Ransom-O’Neill Isolation (ROI)² technique. To briefly outline the process, we achieve ROI by breaking up the pulse times of arrival (TOAs) into temporally bounded groups with piecewise-continuous orbital parameters (O’Neill et al., in prep) to determine local solutions of the orbit at many points over the span of our baseline. We then remove the orbital timing delays from the TOAs in each group, allowing us to mitigate the strong, observation-

¹ Consequently, we acquired observation with both GUPPI and VEGAS on this MJD.

² So initialized by K.A.C. as the upfront work to determine accurate $T_{0,x}$ measurements yields a significant return on investment.

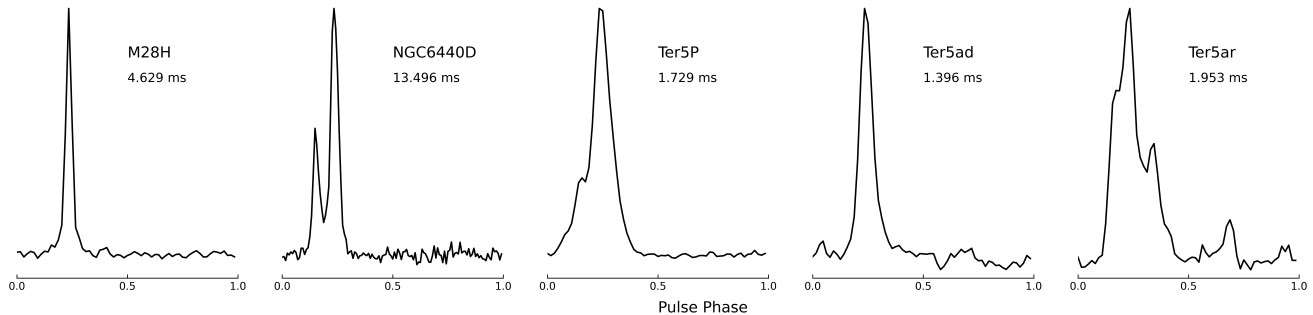


Figure 1. Summed pulse profiles from coherently dedispersed 2 GHz observations for each of the five RBs analyzed in this work.

to-observation variations present in each system. Thus, we effectively “isolate” the underlying MSP clock, which provides us the stability needed to track the rotations of the MSP over the entire baseline (phase-connect) and derive long-term timing solutions for its spin behavior.

3.1. Detections and Initial $T_{0,x}$ Measurements

We first needed to identify all observations for which we had detections of the pulses for each system in our observations. For RBs, this process can be difficult as the T_0 value – the time of passage through periastron, which for our circular ($e = 0$) models is when the MSP crosses the plane of the sky moving away from the observer, called the time of the ascending node – of successive detections can vary dramatically over time. We used SPIDER_TWISTER³ (Ridolfi et al. 2016), which performs searches in orbital phase to return the most probable T_0 value for a given observation, to obtain detections for each source. As our data span roughly 20 years, we automated our searches by allowing SPIDER_TWISTER to search $\pm 10\%$ in orbital phase in the time-series for each observation from its associated T_0 predicted by an initial set of parameters for each system. Even for systems with significant orbital wander, we found this search setup to be effective in finding all available detections in its dataset. We inspected the output plots of each time-series folded at the returned T_0 value⁴ ($T_{0,x}$) and noted non-detections to discard for subsequent steps. At this stage, the $T_{0,x}$ measurements are not necessarily the most accurate value for achieving ROI; however, these measurements are precise enough for obtaining TOAs from each observation. These measurements thus served as an initial set of values that we refined throughout the process (see panel (a) in Figure 2).

³ https://github.com/alex88ridolfi/SPIDER_TWISTER

⁴ We note that $T_{0,x}$ here refers to T_0 for each observation. Herein we generally use this to refer to the T_0 value associated with an arbitrary, binary-piecewise group, x .

3.2. Producing TOAs

We folded the time-series data, using the `prepfold` routine from PRESTO⁵ (Ransom 2001, 2011), for each detection of each MSP using its predicted spin period, DM value, long-term average orbital parameters, and the $T_{0,x}$ measurement for each observation obtained from SPIDER_TWISTER. For Ter5P, Ter5ad, Ter5ar, and M28H, we then integrated over set intervals (10 min for Ter5P and M28H & 30 min for Ter5ad and Ter5ar) to obtain TOAs for each system. Due to the extremely rapid spin periods of Ter5ad and Ter5P, we used separate pulse templates for data obtained in incoherent and coherent dedispersion modes, allowing us to mitigate the effects of smearing for these systems. We visually inspected each fold and noted areas to avoid where there was no pulse (e.g., from both regular and irregular eclipses) as well as areas that may produce erroneous TOAs (e.g., when strong interference was present). We then used PRESTO’s `get_TOAs.py` routine to extract TOAs for each observation in the areas where a signal was present. Finally, we discarded TOAs with errors larger than $30 \mu\text{s}$.

In the case of NGC 6440D, we used the TOAs from Ransom et al. (in prep) with errors less than $30 \mu\text{s}$. These are produced by determining the number of TOAs that could be obtained with sufficient S/N in each observation and integrating over intervals that yield this number of TOAs (roughly 4-15 min integrations). We chose to maintain this slight difference in methodology rather than re-integrating at a set interval to keep the TOAs consistent between both analyses, allowing us to directly compare results obtained via traditional timing techniques to those obtained using the ROI technique.

3.3. Updating Orbital Properties

To ensure that our long-term description of the binary orbital properties was accurate, we used the $T_{0,x}$ values

⁵ <https://github.com/scottransom/presto>

from SPIDER_TWISTER to determine the average orbital period of each system. For all systems except Ter5P and NGC 6440D, we assumed that the period of a circular orbit was constant over the baseline of our observations. We also assumed for all systems that the semi-major axis was constant (see Appendix A for more discussion on these assumptions). We then computed the difference between our measured $T_{0,x}$ value and the value that would be predicted by a constant orbital period and its associated reference epoch $T_{0,\text{ref}}$. With a constant orbital period, these ΔT_0 values over time will show long-term, linear trends if an adjustment to P_b was necessary. We fit a linear trend in these cases as:

$$\frac{\Delta T_0}{t P_b} = \frac{\Delta T_0 f_b}{t} = \frac{\Delta \phi_b}{t}, \quad (1)$$

which describes the change in phase (T_0 in this case) over time, which we used to update the period by computing the change to the orbital frequency via

$$f_{b,\text{new}} = f_{b,\text{old}} + \frac{\Delta T_0}{t} f_{b,\text{old}} \quad (2)$$

and then using

$$P_{b,\text{new}} = \frac{1}{f_{b,\text{new}}}. \quad (3)$$

In the cases of Ter5P and NGC 6440D, the dominant ΔT_0 trend was a quadratic; therefore, we fit both a quadratic and linear term to correct the P_b measurement.

3.4. Constructing Piecewise-Continuous Groups & Parameter Files

For RBs, it is sometimes possible to use a piecewise-discontinuous model to time the system over long baselines, wherein individual chunks of overlapping TOAs spanning some time frame can be strung together with fits using independent models with constant orbital parameters (e.g., Blandford & Teukolsky 1976) to achieve a connected, long-term timing solution (see Rosenthal et al. 2024). A piecewise-continuous, binary model, though, allows for computation of timing residuals for all TOAs over the duration of the baseline with a proper and changing orbit without need for independent fits of other parameters. This process is particularly useful in cases where orbital variations make connecting overlapping chunks difficult. As such, we opted to use the BT_piecewise model (see O’Neill et al., in prep for full details on this model) inside the pulsar timing package, PINT⁶ (Luo et al. 2021) in isolating the TOAs for each

system. While this is not necessary for removing the timing delays described in §3.7, it is useful in predicting how the isolated timing residuals will look with those delays removed.

Using the TOAs from §3.2, we constructed an initial set of piecewise-continuous groups of similar TOAs for each system. We used the TOAs.get_clusters method inside PINT, to identify groups of temporally related TOAs over a specified gap limit. As our datasets contain varying sizes of gaps between observations, we tested a number of different gap limit values using TOAs from Ter5P and Ter5ar by iteratively refining the piecewise groups and $T_{0,x}$ measurements. Ultimately, we found that a gap limit of 0.5 d worked well for most systems to group observations temporally very close together (e.g., two scans on the same day) while not creating groups too temporally large to get an accurate picture of the local solution. Due to the nature of how NGC 6440D’s TOAs were constructed, we used a gap limit of only 0.04166 d to create its piecewise groups as larger gap limit values created some groups with TOAs too sparse to describe the local orbital variations. Once all of the TOAs were assigned a group number, we generated four values for each group that the binary-piecewise model uses to describe local solutions: XR1, XR2, A1X, and TOX, which are the start, finish, $a \sin(i)/c$, and $T_{0,x}$ values, respectively. It is important to note again that we assumed the semi-major axis of the binary is constant over our baseline for these systems.

We then created three different parameter files (or par files) that describe each system – one that describes the local, binary solution of the piecewise groups, another the long-term, binary solution, and finally the isolated, spin behavior. To successfully track the rotations of the pulsar (phase connect) over the full timing baseline, it is helpful (although not strictly necessary) that these three par files be derived from a solution that has some portion of the data phase connected. We initially started with right ascension, declination, the spin frequency and its first derivative from previous short-duration phase connection from Ransom et al. (2005) & Padmanabh et al. (2024) for Ter5 systems, Bégin (2006) for M28H, and Ransom et al. (in prep) for NGC 6440D. We then assumed simple binary models using the P_b , \dot{P}_b (where applicable), and $T_{0,x}$ values as determined in §3.3 to create the binary-piecewise and long-term binary par files. For the isolated par file, which only describes the MSP’s spin, we simply removed the binary information.

3.5. Refining $T_{0,x}$ with TEMPO

As previously stated, the initial measurements of $T_{0,x}$ do not always suffice to accurately describe the behav-

⁶ <https://github.com/nanograv/PINT>

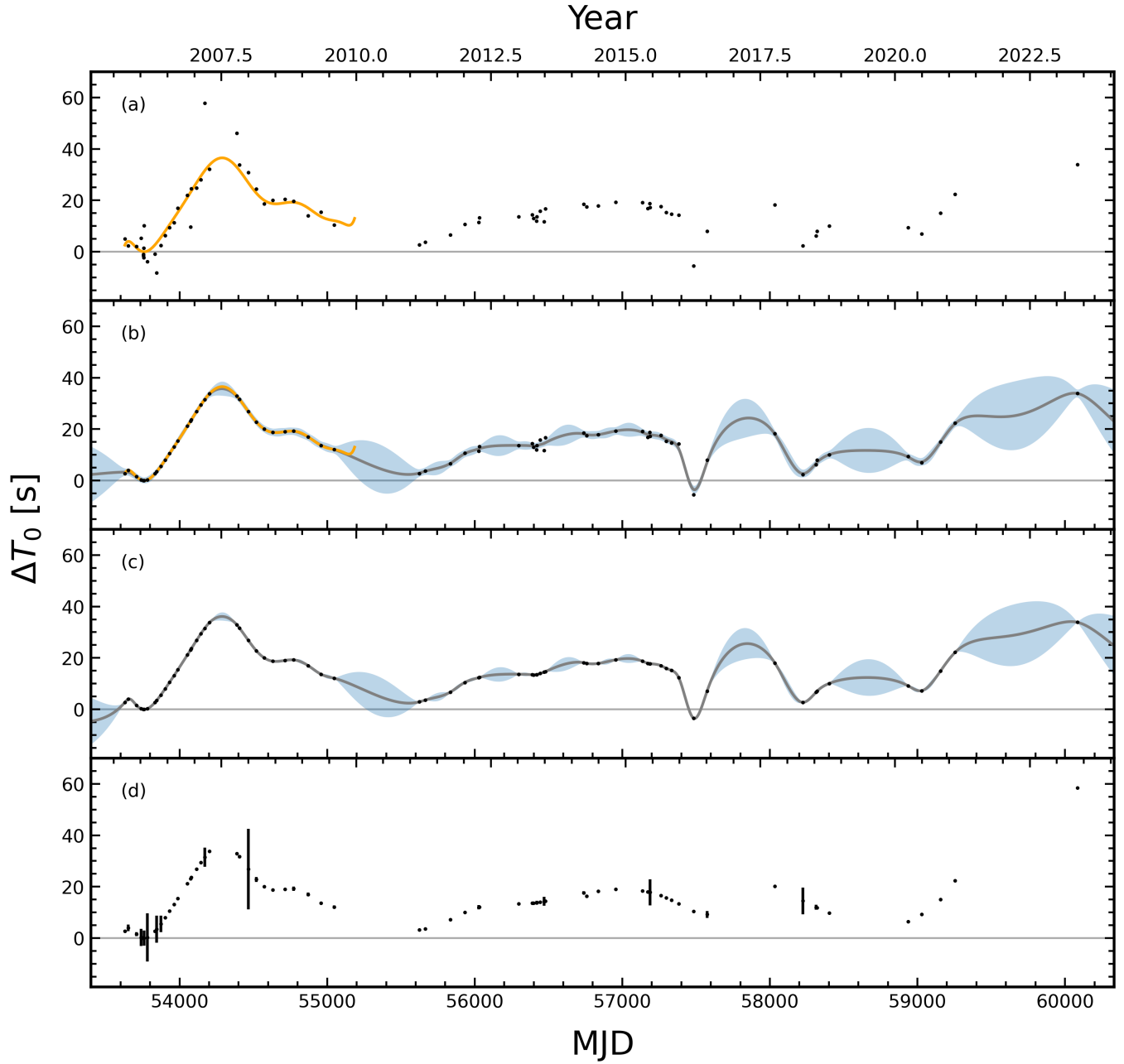


Figure 2. Each panel shows different measurements of time of periastron passage (T_0) deviations over time for M28H as black points. In panel (a), we show the ΔT_0 values derived from the SPIDER_TWISTER values described in §3.1, and we overlay in orange the predicted values from the phase-connected, BTX model described in §3.6. In panel (b), we show the ΔT_0 values accounting for BTX predictions, as well as a Gaussian process regression (GPR) to interpolate between the BTX-informed, T_0 values and the remaining SPIDER_TWISTER measurements. In panel (c), we show the remaining values set to those GPR predictions, as well as a new regression to describe the updated measurements. This process still benefits from manual improvement to ensure ΔT_0 is relatively smooth with time, and we show the resultant values and their errors in panel (d).

ior of each piecewise group. In general, the processes described in the following section are sufficient for correcting the accuracy of each measurement to proceed with the isolation steps. For Ter5P, as well as [Rosen-thal et al.’s \(2024\)](#) work with Ter5A, though, we found that the results of those processes were improved by first refining the $T_{0,x}$ measurements that are used as inputs by fitting T_0 directly to the measured TOAs. To do this, we used [TEMPO⁷](#) and its [TRACK](#) capabilities to fit the TOAs for $T_{0,x}$ in places where the value measured via [SPIDER_TWISTER](#) was not sufficient. In some cases, problematic TOAs that had made it through the initial cleaning stage had caused the initial measurement to be less accurate, while in others, a correction for an improper phase wrap (i.e., pulse count) greatly improved the measurement. The TOX values were then updated in the binary-piecewise par file and used for the final improvement steps.

3.6. Refining $T_{0,x}$ via BTX Information & Gaussian Process Regression

To obtain $T_{0,x}$ measurements that were sufficient to describe the local behavior of each group well, we implemented a two-step process to enhance each value’s accuracy. The first was to bring back some of the information that was discarded in creating the simple-binary model. We used the orbital frequency derivatives from the BTX solutions and phases from [PINT’s](#) `model.orbital_phase` method to compute the orbital period at the current $T_{0,x}$ for each group contained in the original phase-connected solution (see panel (a) in [Figure 2](#)). For systems where we assumed a constant orbital period, which are all but Ter5P and NGC 6440D, this value did not change. These values were the driving force behind the earlier solutions for describing the orbit at all points for that data, so naturally they locally described the TOAs in those portions of our data to a high degree of accuracy. We then updated the $T_{0,x}$ and ΔT_0 values for this subset of the data.

The second step was to use our BTX derived $T_{0,x}$ values, the measured $T_{0,x}$ values for the remaining groups, and both of their corresponding ΔT_0 values as inputs to train a Gaussian process regression (GPR; [Rasmussen & Williams 2006](#)). We used the Matérn kernel implemented in the `scikit-learn` package ([Pedregosa et al. 2011](#)) with an initial length scale of $\ell = 20$, length scale bounds from $1\text{-}10^4$ d, and a white noise kernel with a noise level of 1.5 s and noise bound from $10^{-2}\text{-}10^2$ s. We used the GPR kernel to predict the $T_{0,x}$ values for the

groups not set by the BTX model (see panel (b) in [Figure 2](#)), and we used these values to update each TOX value for the piecewise groups (see panel (c) in [Figure 2](#)). While these values provided great improvement on the accuracy of the $T_{0,x}$ measurements, the quality of the initial measurements were not always such that the GPR arrived at a value that properly described the TOAs local behavior. In these cases, we visually inspected ΔT_0 over time overlaid with the results of the GPR. We exploited the fact that the variation in ΔT_0 over time should be fairly smooth to determine the adjustments (ranging from only a few fractions of a second up to a few 10s of seconds) to the $T_{0,x}$ value needed to correct the local behavior of a group’s TOAs (see panel (d) in [Figure 2](#)). After iteratively refining the GPR, we updated the TOX values for the binary-piecewise model.

3.7. Isolating the MSP

With more refined measurements of $T_{0,x}$, we removed the short- and long-term characteristics of the binary to place each MSP in ROI. For each group in each RB’s binary-piecewise model, we first used [PINT](#) to fit the simple-binary model for only $T_{0,x}$ to get its uncertainty and, in a very small number of cases, updated the $T_{0,x}$ measurement to further improve its accuracy. Next we removed TOAs with orbital phases coincident with a defined eclipse region as described by the simple-binary model, giving us a set of non-eclipsed TOAs, t_i . We then computed the Roemer delays (Δ_R) at t_i based on the simple-binary model, and we created an identical set of TOAs, $t_{\Delta_R,i}$, from which we then remove the Roemer delay. We also needed to apply barycentric to topocentric corrections (β_i) to the predicted Roemer delays, which requires corrections to Δ_R for both t_i and $t_{\Delta_R,i}$ to properly describe an isolated state. To do this we used the simple binary model to compute corrections for the Δ_R corresponding to t_i , β_t , and we used the isolated model to compute corrections for the Δ_R corresponding to $t_{\Delta_R,i}$, β_{Δ_R} , as these TOAs are now in a form of isolation. Using these two terms and Δ_R , we then computed a first-order correction that describes the barycentering effects needed to remove the orbital timing delays from each group, defined as:

$$\beta_i = (\beta_t - \beta_{\Delta_R}) - \Delta_R. \quad (4)$$

We finally removed Δ_R and β_i from t_i . The full sets of TOAs including all of the above corrections then represent the MSP in a state of ROI described by the isolated par file. Tests using simulated binary TOAs reveal that we are able to remove orbital effects to better than 100 ns using this technique.

⁷ <https://tempo.sourceforge.net/>

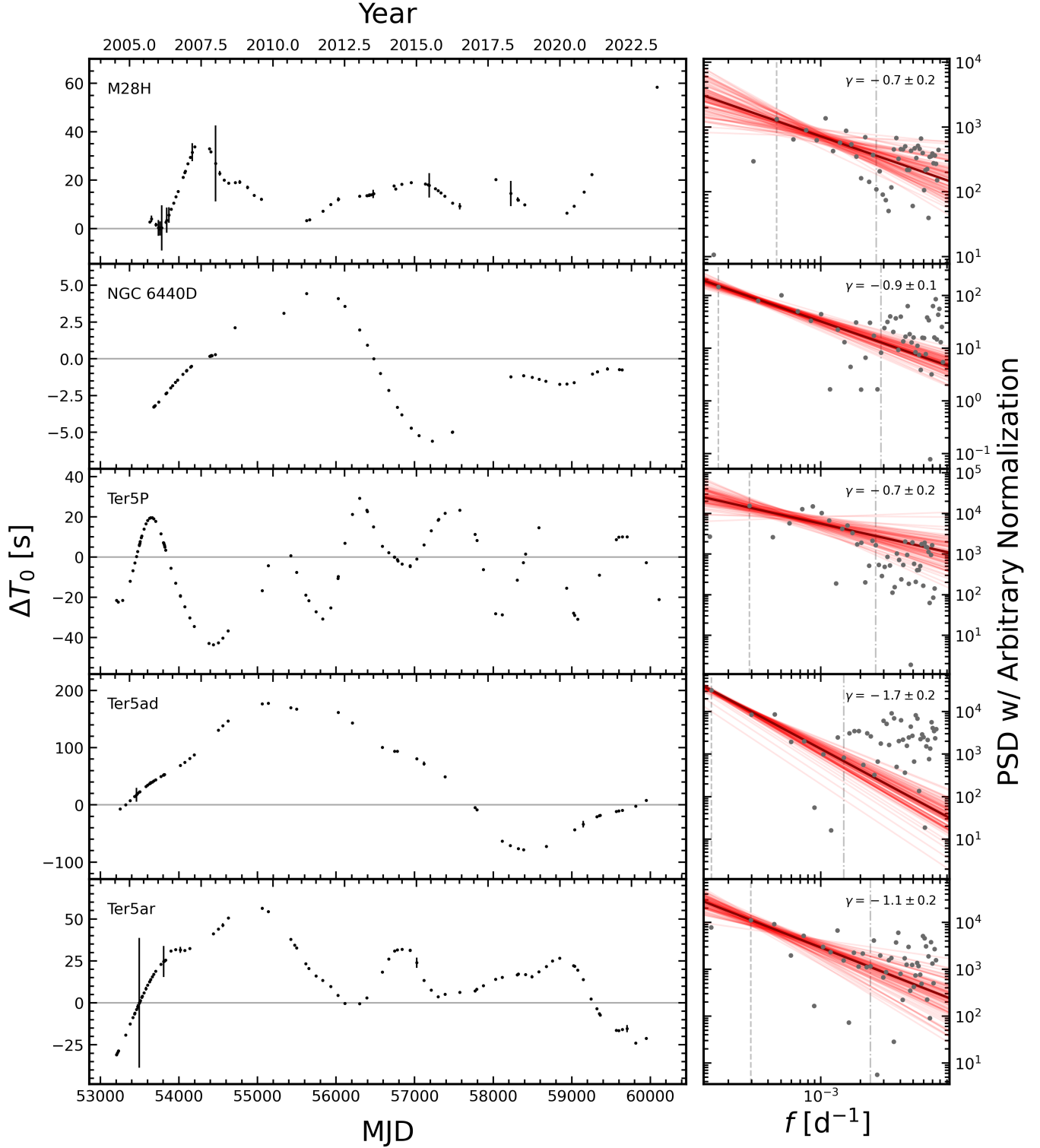


Figure 3. *Left:* As in Figure 2, phase variations (ΔT_0) for each system over time using their final $T_{0,x}$ values. Note that NGC 6440D and Ter5P are shown with their respective P_b 's removed. *Right:* Power Spectral Densities (PSD; grey points) of the ΔT_0 s for each system from a Lomb-Scargle periodogram with an arbitrary normalization. In dark red we show the best fit power-law to the frequencies between the dashed and dash-dotted lines. The γ values and their error for this fit are given in the upper right of each plot. In red, we show a multi-variate gaussian sampling representing the error region of our fit.

3.8. Fitting & Inflating Uncertainties

We performed our fitting for long-term timing parameters like the pulsar spin frequency, frequency derivative, position and proper motion, using PINT. Initially, we use `pintk` – a GUI-based implementation of PINT – with a Downhill weighted least-squares fitter (Susobhanan et al. 2024) to get a preliminary, long-term fit as `pintk` allows for quick changes of various fitting parameters and TOA grouping. We included positions, proper motion in right ascension, DM, frequency, and various numbers of spin frequency derivatives in these fits. Susobhanan et al. (2024) performed various noise parameter tests that show the measured uncertainties on TOAs via fitting algorithms are likely underestimated on their own. They also added noise parameters to the PINT Downhill fitter that can be used to inflate the uncertainties to better describe the measured physical quantities in the fit. We therefore added two fitted error factors (EFACs) to our models – one for the incoherent data and the other for the coherent data – to inflate the errors from our initial fits. This inflation helps to compensate for the systematics due to un-measured and un-modeled DM effects caused by perturbations in the TOAs from the ionized gas in these systems. We chose not to include a fit for errors added in quadrature (e.g., EQUAD) as it may not properly describe the white noise of the isolated TOAs since the initial datasets are dominated by systematics. We then used PINT to perform the final fitting for each system, and we centered the epoch for our measurement of the spin period and the positions along our baseline.

4. RESULTS

4.1. Pulse Profiles

With the exception of Ter5ar, which is the most recently discovered (see Figure 3 in Padmanabh et al. 2024), the previously published pulse profiles for these RBs were only able to make use of the incoherent data available at the time. Furthermore, the coherent data for the Ter5 systems in this work were not analyzed by Martsen et al. (2022) due to the general difficulty in aligning and summing RB profiles – a process aided here by our analysis of the binary orbits. We therefore include summed pulse profiles derived from our coherent dedispersion observations for each MSP in Figure 1. Each profile is a sum of many tens to over 100 hours of S-band, coherent-dedispersion data centered at 2 GHz. Of note, we point out the secondary peak that can be seen in the profile of Ter5P, and we also see a noticeably sharper peak in the profile of Ter5P and Ter5ad than that of their incoherent profile in Ransom et al. (2005) and Hessels et al. (2006).

4.2. Phase Variations

The orbital variations and wander in RBs are a driving force of the systematics in the long-term solutions of each system. Thus, we show in Figure 3 our final measurements of $T_{0,x}$ for the five RBs and how they compare to the value predicted by each simple-binary model over the baseline of each system. These variations represent a large portion of the orbital information removed by the ROI technique. We also show the same variations for Ter5P and NGC 6440D with the \dot{P}_b removed in Figure 5. In §3, we outline how important accurate measurements of $T_{0,x}$ are to effectively understanding these variations and performing subsequent timing; therefore, we include all of the above measurements of $T_{0,x}$ in Table 1.

We also include the power spectral density (PSD) for the T_0 deviations for each system computed using a Lomb-Scargle periodogram (Scargle 1982; Astropy Collaboration et al. 2013, 2018, 2022) in Figure 3. The slope of these PSDs is the spectral index, γ , of the orbital phase variations, meaning it may contain information relating to the underlying mechanisms that drive change to the orbital period. Shown are the results of power-law fits to the frequency bins between the bins partially covariant with \dot{P}_b and the bins associated with white noise. The best-fit γ and its error are shown in the upper right of each plot.

4.3. Long-term Timing Solutions

Timing residuals from our fully-phase-connected timing solutions for the spin behavior of each RB after performing the ROI technique and fitting are shown in Figure 4. The resultant parameters for each system are given in Tables 2 & 3. Despite the significant systematics posed by the orbit and circumbinary material, we are still able to very accurately measure the spin properties of the MSPs over nearly 20 years.

5. DISCUSSION

The success of the ROI technique in allowing for long-term descriptions of MSP spin behavior marks a significant step in the pursuit of timing pulsars in RBs with dramatic orbital variations. Even in the presence of large systematics, this novel method allows us to account for each MSP’s rotation over nearly 20 years.

5.1. Applegate Model Applied to Ter5P

The Applegate mechanism (Applegate 1992) is the most common theory of how variations in a companion star can be used to describe periodic orbital variations in RBs and other compact binaries, and it has been shown to describe at least one eclipsing MSP (e.g., PSR

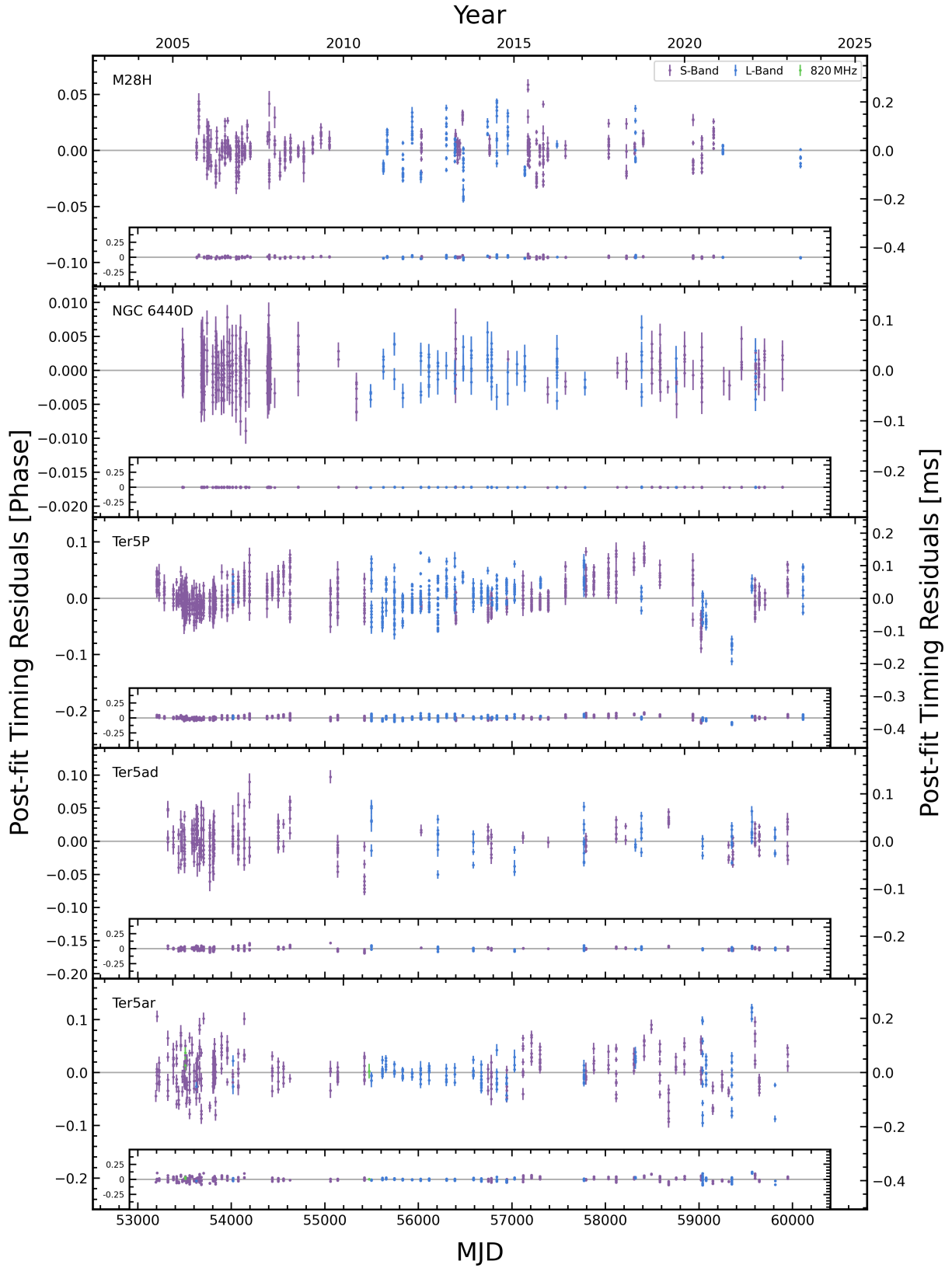


Figure 4. Timing residuals for the five RBs described in this work after applying the ROI technique. We note that the errors shown here are our *measured* uncertainties from §3.7, not the inflated errors used to measure the spin properties in §3.8. Each inset plot shows the same data, but with axes noting ± 0.5 pulse phase to highlight how close to zero the residuals are.

B1957+20, which has a $\Delta P/P = 1.6 \times 10^{-7}$; [Arzoumanian et al. 1994](#); [Applegate & Shaham 1994](#)). In the model, the gravitational quadrupole moment of the companion star can change, perhaps due to magnetic activity, and this can couple with the orbital period and give rise to variations. Examining Figure 5a with the \dot{P}_b removed, it is possible that quasi-periodic oscillations consistent with the Applegate mechanism might be present in the observed variations of Ter5P. We fit a simple sine wave to the portion of the data above MJD=57500, and from this fit we derive a semi-amplitude of 22.4s and P_{mod} of ~ 1033 d. Using Equation 38 in [Applegate \(1992\)](#), this gives $\Delta P/P = 1.6 \times 10^{-6}$. However, it is clear that both the modulation amplitude and period are not constant over the baseline of our observations. It is also plausible that there are additional or even alternative mechanisms (such as the quadrupole moment of the gravity field of the pulsar’s companion) responsible for the variations that are seen here, especially since we removed a large \dot{P}_b value to uncover them. In any case, this appears to be the first spider pulsar to show many cycles of a quasi-periodic oscillation.

5.2. Timing Solutions

The small dispersion in each of the timing residuals in Figure 4 shows that the noise in the orbits of these system does not necessarily strongly affect the clock of the MSP’s spin. Our data are well described by solutions containing astrometry, as well as small numbers of frequency derivatives – where derivatives after \dot{f} are expected due to the accelerations of the cluster ([Phinney 1992, 1993](#); [Freire et al. 2017](#); [Prager et al. 2017](#)). Some of the variations present in the post-fit residuals are almost certainly a manifestation of $T_{0,x}$ values that are still not yet accurate enough to describe the local solution (e.g., the TOAs around MJD ~ 56600 in M28H). It is important to point out that variations caused by other mechanisms are still present in these systems, though. Small duration eclipses will cause issues with the TOAs by affecting the DM value in that observation. Infalling material can also cause a torque on the MSP’s magnetosphere that will affect the spin. These variations are clear in the timing solution for Ter5P (the most dramatic around MJD ~ 59400), where efforts to further improve the local variations as well as additional frequency derivatives in the timing model failed to remove these sharp features. Similar features are also seen in the long-term timing solution of Ter5A ([Rosenthal et al. 2024](#)). A torque from the material would affect the pulsar as a second derivative change in rotational phase:

$$\tau = I \frac{d^2 \phi}{dt^2}. \quad (5)$$

These torques are likely present at small levels in all of our timing solutions, but the exact magnitude and cause of them likely varies greatly system to system. It is not clear whether the torques would be caused by effects from the companion or nearby stars.

5.3. Positions and Proper Motions

We fit for right ascension (α), declination (δ), and the proper motion only in α (μ_α) in all analyses of the isolated TOAs (see §3.8). Initial assessments of fits allowing proper motion in δ (μ_δ) to vary yield nonsensical measurements, likely due to the low ecliptic latitudes $|\beta| \lesssim 3^\circ$ of these globular clusters, where pulsar timing has much less power measuring declination; therefore, we include μ_δ as a fixed value of 0 in our fits. The sensitivity to δ and by extension μ_δ in fits of long baseline TOAs are inherently less precise than those of α for these pulsars, and the large systematics imposed by the phase variations compound to make measurements of μ_δ exceedingly difficult. Future work and additional observations could seek to improve upon this. It is also important to note that the positions of the pulsars analyzed here were already precisely measured, so only one iteration of the ROI technique was necessary. When using this technique to time newer and slower pulsars, the process of the ROI technique would need to be iterated if there is a significant position shift in the timing results to redo the Solar System delay subtraction.

As a consistency check, we compare our positions to those of both radio and X-ray positions for each system where available. M28H has both radio and X-ray ([Vurgun et al. 2022](#)) positions. We cannot draw any conclusions on the consistency with the cited positions as the reported uncertainties are too small to be feasibly correct; however, our α and δ differ from the reported values of $\alpha = 18:24:31.61052125$ & $\delta = -24:52:17.2268378$ by only 0.7 and 760 mas, respectively. Our values are consistent within errors with the reported X-ray positions. [Freire et al. \(2008\)](#) reports radio-timing positions of $\alpha = 17:48:51.64665(7)$ and $\delta = -20:21:07.414(18)$ for NGC 6440D, and our δ value is entirely consistent with that result. Our α is not consistent within errors, but as was the case with M28H, our value differs by only 0.95 mas. Some of the systems in Ter5 have radio positions from [Urquhart et al. \(2020\)](#). Our measurement of both α and δ for Ter5P and Ter5ar are consistent within errors with the reported values (VLA5 and VLA38, respectively). Ter5P and Ter5ad have X-ray positions from [Bogdanov et al. \(2021\)](#) that are consistent within errors with our measured values. [Bahramian et al. \(2020\)](#) report positions for CXOU J174804.63–244645.2, which [Padmanabh et al. \(2024\)](#) identified as being consistent

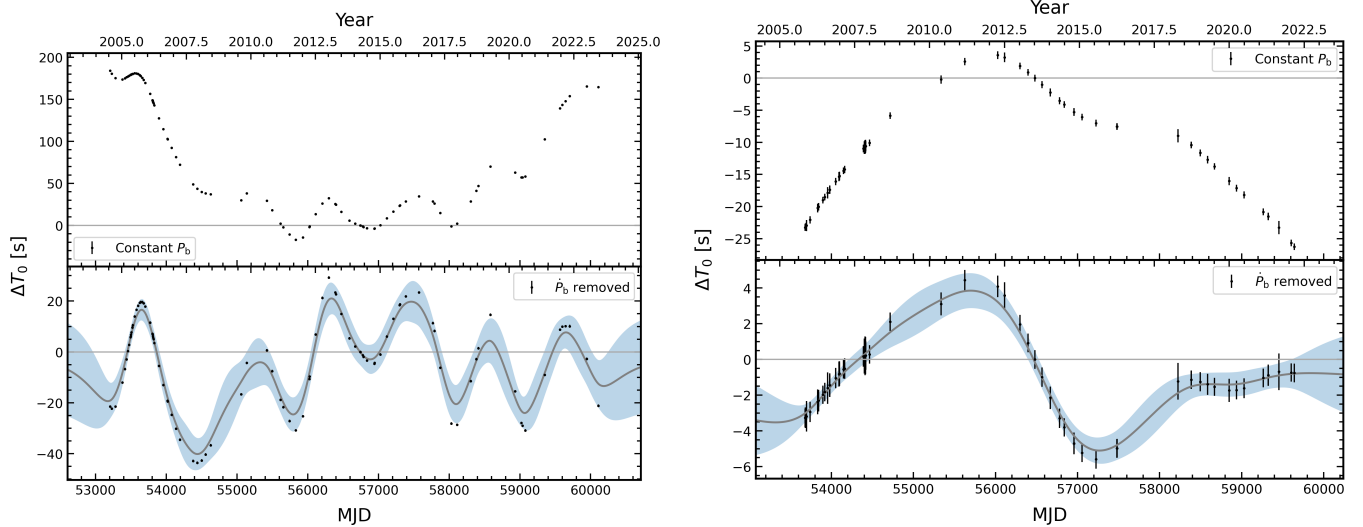


Figure 5. Phase variation (ΔT_0) trends over time for Ter5P (left) and NGC 6440D (right) assuming a constant orbital period (upper panels) and after the removal of the best-fit \dot{P}_b (lower panels). Also shown in the bottom panels are Gaussian process regressions to the measured $T_{0,x}$ values (note these values match those in Figure 3). The quasi-periodic oscillations described in §5.1 for Ter5P are evident.

with Ter5ar. The positions we measure for Ter5ar are not consistent within error with the reported values of $\alpha = 17:48:04.63(13)$ and $\delta = -24:46:45.34(13)$; however, the uncertainties are based off of source extraction via centroiding that may not represent the uncertainties of a dedicated measurement of the X-ray position. Given that our measurements differ by only 10 and 530 mas in α and δ , respectively, it is likely these values would be consistent with uncertainties produced with Hong et al.’s (2005) expression for 95% confidence error circles such as those in Bogdanov et al. (2021).

Similarly, we compared our measured μ_α to those measured for each GC by Vasiliev & Baumgardt (2021) using *Gaia*. The reported values for M28, NGC 6440D, and Ter5 are -0.278 ± 0.028 , -1.187 ± 0.036 , $-1.989 \pm 0.068 \text{ mas yr}^{-1}$, respectively. As shown in Tables 2 & 3, our measurements for NGC 6440D and Ter5ad are consistent within errors with the reported values, while our measurements for M28H, Ter5P, and Ter5ar are not. These values are relatively reasonable given the proper motions of stars in the cluster within an order of magnitude or two, though, and our measurement for Ter5P only differs by $0.189 \text{ mas yr}^{-1}$. As with μ_δ , our measurements of μ_α are likely substantially affected by the systematics of the phase variations. The relative closeness of our measurements are a sign that improvements to the ROI technique in the future may yield accurate μ_α measurements.

5.4. ROI Timing vs. Traditional Timing

In Figure 6 we show a comparison of our long-term timing solution for NGC 6440D created via ROI and the long-term timing solution from Ransom et al. (in prep). The latter solution contains nine orbital frequency derivatives conventionally used for timing. NGC 6440D is by many measures the most well-behaved of the systems in our sample, having orbital variations with far less drastic effects on the observations. The results of both methods look to be nearly identical, which is a useful check on the efficacy of the ROI technique.

We stress that this is not to say that conventional timing techniques should not be used to derive long-term solutions for RBs. Rather we highlight that for systems with significant orbital variations there are useful benefits that our technique provides over conventional methods. Conventional-timing techniques necessitate P_b and nine orbital frequency derivatives to describe the binary effects of NGC 6440D and the effects of the cluster, whereas the ROI technique produces nearly identical results with a simple model to remove binary information entirely. Similarly, higher-order, orbital frequency derivatives poorly predict orbital behavior in large gaps between observations, while the stable spin of the MSP – the connecting factor in our method – extrapolates nicely over those same gaps. Thus, the ROI technique produces nearly identical results by trading orbital frequency derivatives for a number of individual, well-measured $T_{0,x}$ values needed to accurately describe the long-term timing behavior of the systems.

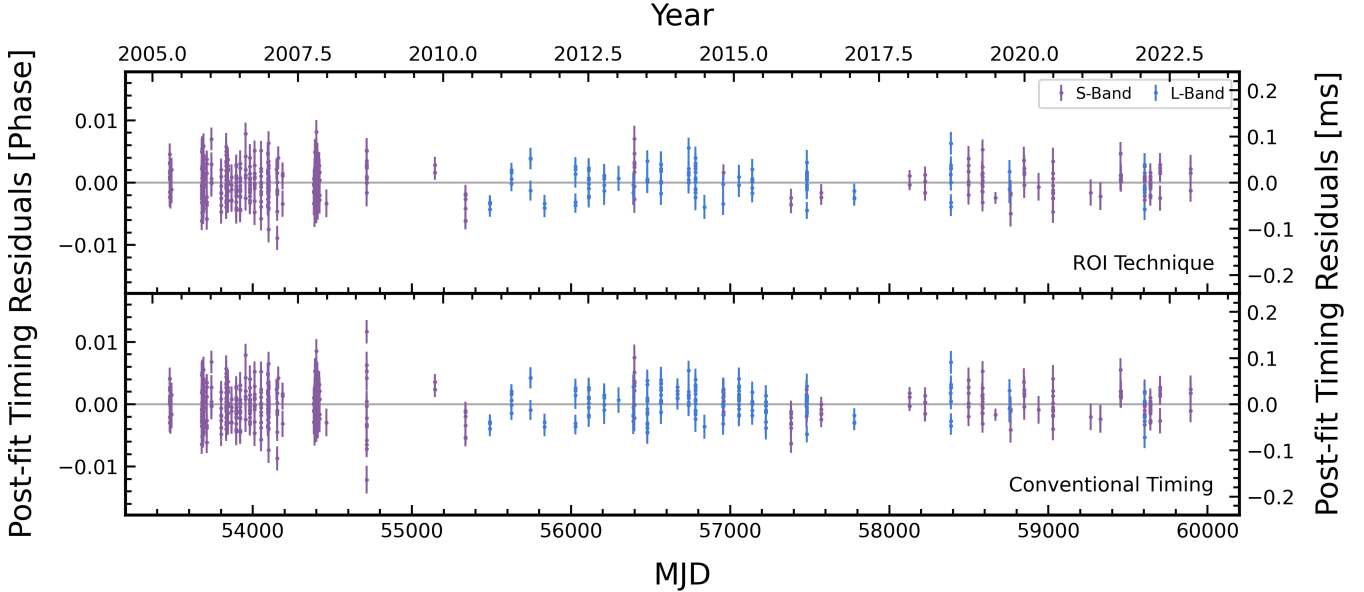


Figure 6. Comparison of timing residuals obtained via the ROI technique (top) and those obtained using conventional timing techniques (bottom). It is clear that these two methods yield nearly identical results.

5.5. Phase Variation Analyses

We analyze a small set of parameters to search for any potential covariances that could yield insights into the phase variations seen in RBs. First, we inspected our γ values, by comparing them against the spin frequency and period, P_b , and semi-major axis for each system. We see no evidence of covariance in any of these parameters. However, as shown in the left panel of Figure 7, it is of note that our γ values are all greater than those of the three systems presented in [Thongmeearkom et al. \(2024\)](#), which have $\gamma < -2.4$, $\gamma = -3.81^{+0.32}_{-0.48}$, and $\gamma < -5.4$, but similar to the $\gamma = -0.9 \pm 0.2$ for Ter5A from [Rosenthal et al. \(2024\)](#). This may simply mean that the observed variations in our systems may not exist in a power-law regime.

We also inspected the standard deviation of the phase variations ($\sigma_{\Delta T_0}$) as a fraction of the orbital period. This experiment was to see if, fractionally, the observed variations were similar or if some systems have higher variations than others. In the four, rightmost plots of Figure 7, we show the fractional deviation ($\sigma_{\Delta T_0}/P_b$) plotted against spin frequency and period, P_b , and semi-major axis. Immediately evident was the correlation $\sigma_{\Delta T_0}/P_b$ has with spin frequency (and inversely with spin period) and potentially with the projected semi-major axis. Although there is more noise in the trend, it is clear that, as the binary distance tightens, the fractional deviation in the phase variations becomes less drastic. The near direct relationship with spin frequency is certainly the most striking.

It is unclear what the physical mechanism for this relationship would be. Younger MSPs that have just been spun up by their binary companion may have the fastest spins and be closer to the point where they overflowed their Roche lobe to contribute the material for spinning up the pulsar. This could mean more material would be present to perturb the system, more interactions would be taking place as the pulsar finishes its spin up, or both. Older and slower MSPs would be then be farther from this evolutionary stage and more settled, and thus may not be prone to large variations. Owing to the precise nature of the ROI technique, it is possible that this is a manifestation of the sensitivity of our $T_{0,x}$ measurements, where the more rapidly a system is rotating, the more accurate the values of $T_{0,x}$ need to be. Future long-term studies of these systems may be able to disentangle the physical reasoning behind these strong trends, assuming they are not byproducts of small statistics.

5.6. Mitigating Systematics in the Future

As has been mentioned throughout the text, there are systematics present in these datasets that serve as contaminants. We are able to remove a good portion of them through the ROI technique; however, it is not to be assumed that all systematics have been removed at this point. While it is likely not possible to account for every variation caused by the eclipses, gas in the system, or any torques imposed by accreted material, finding more ways to even further improve the $T_{0,x}$ measurement for a piecewise group can in fact go a long way to mitigate local systematics. One simple addition to the ROI tech-

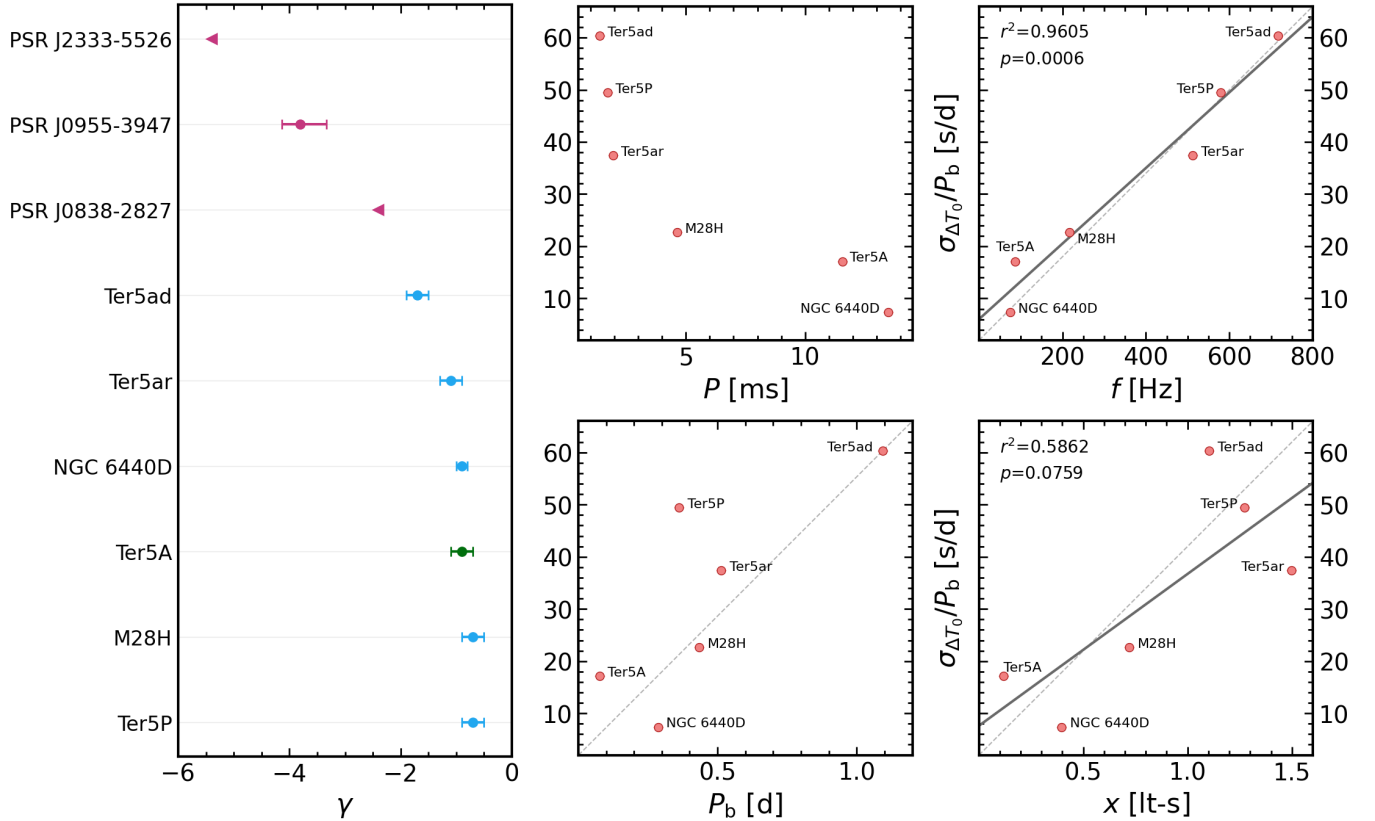


Figure 7. *Left:* All currently measured γ values for RBs. Values from this work are shown in blue, the value for Ter5A from Rosenthal et al. (2024) is shown in green, and the three values from Thongmeekom et al. (2024) are shown in pink. Upper limits are plotted as triangles. *Right:* The fractional deviation of the five RBs described here, as well as Ter5A, plotted against spin period (upper left), spin frequency (upper right), orbital period (bottom left), and projected semi-major axis (bottom right). Values for Ter5A come from analysis presented in Rosenthal et al. (2024). Also plotted as a solid line is a linear regression fit for the strong correlation seen with spin frequency and the weaker one with projected semi-major axis, as well as the regression’s r^2 and p -values. The light-gray, dashed lines in each plot show the one-to-one line for that variable.

nique for future studies could be to implement a simple routine that finds a $T_{0,x}$ that both minimizes the dispersion of TOAs in post-fit phase and keeps the group close to a long-term trend line of the isolated TOAs. We also reiterate that our analysis was conducted using time-series data, as it keeps the problem at hand far simpler to address. Future studies will be able to leverage the multi-frequency information of raw data to account for DM variations and delays in certain observations. These variations are likely some of the largest contaminants to measurements of $T_{0,x}$, and our analysis of the time-series data only removes a small fraction of them by removing TOAs near the eclipse.

6. SUMMARY

We have presented a novel technique for “isolating” the underlying MSP clock in binaries with dramatic orbital variations by removing the timing delays from the binary orbit and fitting local variations in the TOAs. This technique allows for phase connection over baselines that

far surpass those of the initial solutions containing binary information. We used this technique to get timing solutions for five RB systems found in three GCs spanning almost two decades. The results of our solutions derived from isolated TOAs are consistent with those derived from conventional timing techniques for GC pulsars, meaning this is an effective alternative for systems that show large phase variations. Variations seen in the five systems we investigated show the broad spectrum of systematics present in RBs, ranging from relatively well behaved (e.g., NGC 6440D) to quasi-periodic (e.g., Ter5P) to unpredictable (e.g., M28H & Ter5ar). An analysis of Ter5P shows that it is possible that its oscillations arise from the Applegate mechanism; however, the changing nature of the oscillations may necessitate additional or alternative mechanisms to fully describe the phase variations. A striking correlation exists between the standard deviation of a system’s variations as a fraction of its orbital period and its spin frequency. Whether this is a probe of the MSPs age since being

spun up, the inherent susceptibility of an MSP to perturbations based on its spin, or even just a manifestation of the need for duly accurate measurements of phase, it is clear that future studies of RBs will need to continue this investigation. The nature of RB timing is riddled with pervasive systematics that limit our ability to describe these systems in ways other MSP binaries can be over similar baselines. With refinement to the ROI technique, multi-frequency information, and more systems with long baselines, though, it is still possible to investigate interesting physics problems with these unique binaries.

ACKNOWLEDGEMENTS

The Green Bank Observatory is a facility of the National Science Foundation operated under cooperative

agreement by Associated Universities, Inc. The National Radio Astronomy Observatory is a facility of the National Science Foundation operated under cooperative agreement by Associated Universities, Inc.

Support for this work was provided to K.A.C. by the NSF through the Grote Reber Fellowship Program administered by Associated Universities, Inc./National Radio Astronomy Observatory. S.M.R. is a CIFAR Fellow and is supported by the NSF Physics Frontiers Center awards 2020265. Pulsar research at UBC is supported by an NSERC Discovery Grant and by the Canadian Institute for Advanced Research.

We would like to acknowledge Brian Prager for his part in presenting some of the equations found in Appendix A.

REFERENCES

- Abbate, F., Possenti, A., Ridolfi, A., et al. 2018, *MNRAS*, 481, 627, doi: [10.1093/mnras/sty2298](https://doi.org/10.1093/mnras/sty2298)
- Alpar, M. A., Cheng, A. F., Ruderman, M. A., & Shaham, J. 1982, *Nature*, 300, 728, doi: [10.1038/300728a0](https://doi.org/10.1038/300728a0)
- Applegate, J. H. 1992, *ApJ*, 385, 621, doi: [10.1086/170967](https://doi.org/10.1086/170967)
- Applegate, J. H., & Shaham, J. 1994, *ApJ*, 436, 312, doi: [10.1086/174906](https://doi.org/10.1086/174906)
- Archibald, A. M., Kaspi, V. M., Hessels, J. W. T., et al. 2013, arXiv e-prints, arXiv:1311.5161, doi: [10.48550/arXiv.1311.5161](https://doi.org/10.48550/arXiv.1311.5161)
- Arzoumanian, Z., Fruchter, A. S., & Taylor, J. H. 1994, *ApJL*, 426, L85, doi: [10.1086/187346](https://doi.org/10.1086/187346)
- Astropy Collaboration, Robitaille, T. P., Tollerud, E. J., et al. 2013, *A&A*, 558, A33, doi: [10.1051/0004-6361/201322068](https://doi.org/10.1051/0004-6361/201322068)
- Astropy Collaboration, Price-Whelan, A. M., Sipőcz, B. M., et al. 2018, *AJ*, 156, 123, doi: [10.3847/1538-3881/aabc4f](https://doi.org/10.3847/1538-3881/aabc4f)
- Astropy Collaboration, Price-Whelan, A. M., Lim, P. L., et al. 2022, *ApJ*, 935, 167, doi: [10.3847/1538-4357/ac7c74](https://doi.org/10.3847/1538-4357/ac7c74)
- Bahramian, A., Strader, J., Miller-Jones, J. C. A., et al. 2020, *ApJ*, 901, 57, doi: [10.3847/1538-4357/aba51d](https://doi.org/10.3847/1538-4357/aba51d)
- Bégin, S. 2006, Master's thesis, University of British Columbia, Canada
- Bellm, E. C., Kaplan, D. L., Breton, R. P., et al. 2016, *ApJ*, 816, 74, doi: [10.3847/0004-637X/816/2/74](https://doi.org/10.3847/0004-637X/816/2/74)
- Bilous, A. V., Ransom, S. M., & Demorest, P. 2019, *ApJ*, 877, 125, doi: [10.3847/1538-4357/ab16dd](https://doi.org/10.3847/1538-4357/ab16dd)
- Blandford, R., & Teukolsky, S. A. 1976, *ApJ*, 205, 580, doi: [10.1086/154315](https://doi.org/10.1086/154315)
- Bogdanov, S., Bahramian, A., Heinke, C. O., et al. 2021, *ApJ*, 912, 124, doi: [10.3847/1538-4357/abee78](https://doi.org/10.3847/1538-4357/abee78)
- Bogdanov, S., van den Berg, M., Servillat, M., et al. 2011, *ApJ*, 730, 81, doi: [10.1088/0004-637X/730/2/81](https://doi.org/10.1088/0004-637X/730/2/81)
- Clark, C. J., Nieder, L., Voisin, G., et al. 2021, *MNRAS*, 502, 915, doi: [10.1093/mnras/staa3484](https://doi.org/10.1093/mnras/staa3484)
- Deneva, J. S., Ray, P. S., Camilo, F., et al. 2021, *ApJ*, 909, 6, doi: [10.3847/1538-4357/abd7a1](https://doi.org/10.3847/1538-4357/abd7a1)
- DuPlain, R., Ransom, S., Demorest, P., et al. 2008, in Society of Photo-Optical Instrumentation Engineers (SPIE) Conference Series, Vol. 7019, *Advanced Software and Control for Astronomy II*, ed. A. Bridger & N. M. Radziwill, 70191D, doi: [10.1117/12.790003](https://doi.org/10.1117/12.790003)
- Fonseca, E., Cromartie, H. T., Pennucci, T. T., et al. 2021, *ApJL*, 915, L12, doi: [10.3847/2041-8213/ac03b8](https://doi.org/10.3847/2041-8213/ac03b8)
- Freire, P. C. C. 2013, in *Neutron Stars and Pulsars: Challenges and Opportunities after 80 years*, ed. J. van Leeuwen, Vol. 291, 243–250, doi: [10.1017/S1743921312023770](https://doi.org/10.1017/S1743921312023770)
- Freire, P. C. C., Ransom, S. M., Bégin, S., et al. 2008, *ApJ*, 675, 670, doi: [10.1086/526338](https://doi.org/10.1086/526338)
- Freire, P. C. C., & Wex, N. 2024, *Living Reviews in Relativity*, 27, 5, doi: [10.1007/s41114-024-00051-y](https://doi.org/10.1007/s41114-024-00051-y)
- Freire, P. C. C., Ridolfi, A., Kramer, M., et al. 2017, *MNRAS*, 471, 857, doi: [10.1093/mnras/stx1533](https://doi.org/10.1093/mnras/stx1533)
- Ghosh, A., Bhattacharyya, B., Lyne, A., et al. 2024, *ApJ*, 965, 64, doi: [10.3847/1538-4357/ad31ab](https://doi.org/10.3847/1538-4357/ad31ab)
- Hessels, J. W. T., Ransom, S. M., Stairs, I. H., et al. 2006, *Science*, 311, 1901, doi: [10.1126/science.1123430](https://doi.org/10.1126/science.1123430)
- Hong, J., van den Berg, M., Schlegel, E. M., et al. 2005, *ApJ*, 635, 907, doi: [10.1086/496966](https://doi.org/10.1086/496966)
- Kaplan, D. L., Escoffier, R. P., Lacasse, R. J., et al. 2005, *PASP*, 117, 643, doi: [10.1086/430368](https://doi.org/10.1086/430368)

- Kramer, M., Stairs, I. H., Manchester, R. N., et al. 2021, *Physical Review X*, 11, 041050, doi: [10.1103/PhysRevX.11.041050](https://doi.org/10.1103/PhysRevX.11.041050)
- Luo, J., Ransom, S., Demorest, P., et al. 2021, *ApJ*, 911, 45, doi: [10.3847/1538-4357/abe62f](https://doi.org/10.3847/1538-4357/abe62f)
- Lyne, A. G., Manchester, R. N., D'Amico, N., et al. 1990, *Nature*, 347, 650, doi: [10.1038/347650a0](https://doi.org/10.1038/347650a0)
- Manchester, R. N., Hobbs, G. B., Teoh, A., & Hobbs, M. 2005, *AJ*, 129, 1993, doi: [10.1086/428488](https://doi.org/10.1086/428488)
- Martsen, A. R., Ransom, S. M., DeCesar, M. E., et al. 2022, *ApJ*, 941, 22, doi: [10.3847/1538-4357/aca156](https://doi.org/10.3847/1538-4357/aca156)
- Miraval Zanon, A., Burgay, M., Possenti, A., & Ridolfi, A. 2018, in *Journal of Physics Conference Series*, Vol. 956, *Journal of Physics Conference Series (IOP)*, 012004, doi: [10.1088/1742-6596/956/1/012004](https://doi.org/10.1088/1742-6596/956/1/012004)
- Nice, D. J., Arzoumanian, Z., & Thorsett, S. E. 2000, in *Astronomical Society of the Pacific Conference Series*, Vol. 202, *IAU Colloq. 177: Pulsar Astronomy - 2000 and Beyond*, ed. M. Kramer, N. Wex, & R. Wielebinski, 67, doi: [10.48550/arXiv.astro-ph/9911211](https://doi.org/10.48550/arXiv.astro-ph/9911211)
- Nice, D. J., Thorsett, S. E., Taylor, J. H., & Fruchter, A. S. 1990, *ApJL*, 361, L61, doi: [10.1086/185827](https://doi.org/10.1086/185827)
- Padmanabh, P. V., Ransom, S. M., Freire, P. C. C., et al. 2024, *A&A*, 686, A166, doi: [10.1051/0004-6361/202449303](https://doi.org/10.1051/0004-6361/202449303)
- Pallanca, C., Dalessandro, E., Ferraro, F. R., et al. 2010, *ApJ*, 725, 1165, doi: [10.1088/0004-637X/725/1/1165](https://doi.org/10.1088/0004-637X/725/1/1165)
- Papitto, A., Ferrigno, C., Bozzo, E., et al. 2013, *Nature*, 501, 517, doi: [10.1038/nature12470](https://doi.org/10.1038/nature12470)
- Predregosa, F., Varoquaux, G., Gramfort, A., et al. 2011, *Journal of Machine Learning Research*, 12, 2825
- Phinney, E. S. 1992, *Philosophical Transactions of the Royal Society of London Series A*, 341, 39, doi: [10.1098/rsta.1992.0084](https://doi.org/10.1098/rsta.1992.0084)
- Phinney, E. S. 1993, in *Astronomical Society of the Pacific Conference Series*, Vol. 50, *Structure and Dynamics of Globular Clusters*, ed. S. G. Djorgovski & G. Meylan, 141
- Polzin, E. J., Breton, R. P., Stappers, B. W., & LOFAR PWG. 2018, in *Pulsar Astrophysics the Next Fifty Years*, ed. P. Weltevrede, B. B. P. Perera, L. L. Preston, & S. Sanidas, Vol. 337, 396–397, doi: [10.1017/S1743921317009115](https://doi.org/10.1017/S1743921317009115)
- Prager, B. J. 2017, PhD thesis, University of Virginia
- Prager, B. J., Ransom, S. M., Freire, P. C. C., et al. 2017, *ApJ*, 845, 148, doi: [10.3847/1538-4357/aa7ed7](https://doi.org/10.3847/1538-4357/aa7ed7)
- Prestage, R. M., Bloss, M., Brandt, J., et al. 2015, in 2015 URSI-USNC Radio Science Meeting, 4, doi: [10.1109/USNC-URSI.2015.7303578](https://doi.org/10.1109/USNC-URSI.2015.7303578)
- Ransom, S. 2011, PRESTO: Pulsar Exploration and Search TOolkit, Astrophysics Source Code Library, record ascl:1107.017
- Ransom, S. M. 2001, PhD thesis, Harvard University, Massachusetts
- Ransom, S. M. 2008, in *Dynamical Evolution of Dense Stellar Systems*, ed. E. Vesperini, M. Giersz, & A. Sills, Vol. 246, 291–300, doi: [10.1017/S1743921308015810](https://doi.org/10.1017/S1743921308015810)
- Ransom, S. M., Hessels, J. W. T., Stairs, I. H., et al. 2005, *Science*, 307, 892, doi: [10.1126/science.1108632](https://doi.org/10.1126/science.1108632)
- Rasmussen, C. E., & Williams, C. K. I. 2006, *Gaussian Processes for Machine Learning*
- Ridolfi, A., Freire, P. C. C., Torne, P., et al. 2016, *MNRAS*, 462, 2918, doi: [10.1093/mnras/stw1850](https://doi.org/10.1093/mnras/stw1850)
- Roberts, M. S. E. 2013, in *Neutron Stars and Pulsars: Challenges and Opportunities after 80 years*, ed. J. van Leeuwen, Vol. 291, 127–132, doi: [10.1017/S174392131202337X](https://doi.org/10.1017/S174392131202337X)
- Rosenthal, A. C., Ransom, S. M., Corcoran, K. A., et al. 2024, arXiv e-prints, arXiv:2410.21648, doi: [10.48550/arXiv.2410.21648](https://doi.org/10.48550/arXiv.2410.21648)
- Scargle, J. D. 1982, *ApJ*, 263, 835, doi: [10.1086/160554](https://doi.org/10.1086/160554)
- Strader, J., Swihart, S., Chomiuk, L., et al. 2019, *ApJ*, 872, 42, doi: [10.3847/1538-4357/aafbaa](https://doi.org/10.3847/1538-4357/aafbaa)
- Susobhanan, A., Kaplan, D., Archibald, A., et al. 2024, arXiv e-prints, arXiv:2405.01977, doi: [10.48550/arXiv.2405.01977](https://doi.org/10.48550/arXiv.2405.01977)
- Tauris, T. M., & van den Heuvel, E. P. J. 2006, in *Compact stellar X-ray sources*, Vol. 39, 623–665, doi: [10.48550/arXiv.astro-ph/0303456](https://doi.org/10.48550/arXiv.astro-ph/0303456)
- Tauris, T. M., & van den Heuvel, E. P. J. 2023, *Physics of Binary Star Evolution. From Stars to X-ray Binaries and Gravitational Wave Sources*, doi: [10.48550/arXiv.2305.09388](https://doi.org/10.48550/arXiv.2305.09388)
- Thongmearkom, T., Clark, C. J., Breton, R. P., et al. 2024, *MNRAS*, 530, 4676, doi: [10.1093/mnras/stae787](https://doi.org/10.1093/mnras/stae787)
- Urquhart, R., Bahramian, A., Strader, J., et al. 2020, *ApJ*, 904, 147, doi: [10.3847/1538-4357/abb6fc](https://doi.org/10.3847/1538-4357/abb6fc)
- Vasiliev, E., & Baumgardt, H. 2021, *MNRAS*, 505, 5978, doi: [10.1093/mnras/stab1475](https://doi.org/10.1093/mnras/stab1475)
- Vurgun, E., Linares, M., Ransom, S., et al. 2022, *ApJ*, 941, 76, doi: [10.3847/1538-4357/ac9ea0](https://doi.org/10.3847/1538-4357/ac9ea0)
- Yap, Y. X. J., Kong, A. K. H., & Li, K.-L. 2023, *ApJ*, 955, 21, doi: [10.3847/1538-4357/acea82](https://doi.org/10.3847/1538-4357/acea82)
- You, X. P., Manchester, R. N., Coles, W. A., Hobbs, G. B., & Shannon, R. 2018, *ApJ*, 867, 22, doi: [10.3847/1538-4357/aadee0](https://doi.org/10.3847/1538-4357/aadee0)

APPENDIX

A. DYNAMICAL CONSIDERATIONS

In this work, we have assumed that the dominant systematic in our timing analysis is changes to the time of periastron passage (i.e., ΔT_0). Empirically, this assumption yields good results, and the addition of DM effect modeling in future implementations will further improve the method's performance. However, from a dynamics perspective, it is unclear if ΔT_0 can be the sole orbital element responsible for observed timing variations. In the text that follows, we outline some dynamical considerations that could be useful in investigating this further. For additional commentary detailing how some equations here relate to studies of MSPs in GCs, see [Prager \(2017\)](#) when they are originally presented.

A.1. Relating T_0 to P_b & \dot{P}_b

For investigations of the orbital period, we relate changes in orbital phase to changes in T_0 as follows:

$$\Delta\phi = n\Delta T_0 = \frac{2\pi}{P_b}\Delta T_0, \quad (\text{A1})$$

where n is the orbital frequency ($n = 2\pi/P_b$). When considering a changing orbital period, we can similarly express the change in orbital phase in terms of:

$$\Delta\phi = \frac{1}{2}\dot{n}\Delta t^2 = \frac{-\pi\dot{P}_b}{P_b^2}(\Delta t)^2, \quad (\text{A2})$$

which relates the characteristic change in P_b to the observed T_0 wander over the timescale Δt through

$$\frac{\Delta P_b}{P_b} \sim 2\frac{\Delta T_0}{\Delta t}. \quad (\text{A3})$$

The characteristic orbital period derivative is then:

$$\dot{P}_b \simeq \frac{\Delta P_b}{\Delta t} = 2P_b\frac{\Delta T_0}{(\Delta t)^2}. \quad (\text{A4})$$

A.2. Relating T_0 to x

For our analyses, we assumed that the semi-major axis is constant over the duration of our baseline, attributing all orbital changes to the time of periastron passage, T_0 . For investigations interested in exploring this assumption, we give a relationship between the T_0 and the projected-semi-major axis, x . From Kepler's third law, the shrinking of the pulsar orbit by gravitational wave damping relates the change in x to P_b as:

$$\frac{\dot{x}}{x} = \frac{2}{3}\frac{\dot{P}_b}{P_b}. \quad (\text{A5})$$

Replacing \dot{P}_b with the result of Equation [A4](#), this becomes:

$$\dot{x} = \frac{4}{3}x\frac{\Delta T_0}{(\Delta t)^2}. \quad (\text{A6})$$

Similarly to \dot{P}_b , the characteristic change in x is then:

$$\dot{x} = \frac{4}{3}x\frac{\Delta T_0}{(\Delta t)^2} \simeq \frac{\Delta x}{\Delta t}. \quad (\text{A7})$$

Rearranging Equation [A7](#), we get the relationship:

$$\Delta T_0 \simeq \frac{3}{4}\frac{\Delta t}{x}\Delta x. \quad (\text{A8})$$

B. SUPPLEMENTARY TABLES

Included here are tables for data and fits used throughout the text. In Table 1 we provide the $T_{0,x}$ values used for our binary-piecewise groups. These values are by no means final for any one group, as improvement in the accuracy of these values is an ever-ongoing process. They should be taken as a more-refined starting place for future analyses of these systems. In Tables 2 and 3 we provide all of the binary information used to remove the orbital timing delays from each system as well as the parameters from our timing models of the spin behaviors.

Table 1. The final measurements of $T_{0,x}$ used in constructing the piecewise-continuous groups for each system.

Group	M28H	NGC 6440D	Ter5P	Ter5ad	Ter5ar
#	T_0 [MJD]				
1	53629.9385207(54)	53478.316129(25)	53204.18393645(17)	53252.23546037(89)	53205.2380510(25)
2	53651.254881(15)	53483.179297(65)	53227.39148316(39)	53320.0901308(32)	53206.26472831(87)
3	53707.8084219(91)	53489.47281(14)	53282.1468202(12)	53379.189373(13)	53216.01816206(60)
4	53739.130384(38)	53679.99454845(94)	53378.9659555(14)	53435.005329(14)	53227.3116125(11)
5	53753.9213147(12)	53681.7109605(15)	53415.22782516(67)	53457.98837(14)	53229.3649678(18)
6	53755.66142441(40)	53681.9970292(34)	53439.1606633(14)	53474.404824(18)	53320.22591517(53)
7	53756.9665067(91)	53683.7134413(18)	53459.1046954(14)	53495.1990014(10)	53379.7732062(12)
8	53757.8365616(17)	53685.7159220(16)	53475.0599204(36)	53500.6711532(16)	53414.68023902(50)
9	53759.141644(34)	53687.718403(22)	53493.55347757(39)	53579.4701322(44)	53434.7004489(65)
10	53781.76307(11)	53690.8651583(19)	53496.0918081(11)	53601.3587350(14)	53438.80715862(55)
11	53832.6613151(60)	53696.0143945(81)	53500.44323289(24)	53625.4361957(17)	53458.82736894(93)
12	53844.407066(61)	53709.745691(40)	53506.60775125(21)	53637.474927(36)	53474.227529(17)
13	53872.683875(37)	53709.745691(37)	53520.02464341(23)	53637.474927(18)	53493.73439988(96)
14	53902.26577032(74)	53740.6411085(32)	53526.55177969(20)	53659.3635263(19)	53496.30109(45)
15	53932.28269427(72)	53801.287669(62)	53553.38555898(27)	53679.0632656(20)	53501.43448085(78)
16	53962.2996186(11)	53801.573737(28)	53579.8567112(11)	53703.1407239(22)	53506.5678671(16)
17	53987.96626479(88)	53833.3273607(56)	53601.25119817(40)	53769.9009444(12)	53507.5945451(28)
18	54052.78542310(77)	53833.6134294(31)	53625.18400663(33)	53803.8282678(13)	53526.5880762(13)
19	54074.9718466(11)	53843.3397645(39)	53638.6008805(18)	53804.9226976(22)	53533.77481757(78)
20	54079.75715425(75)	53865.367053(39)	53659.63273154(84)	53806.017127(11)	53554.30836398(40)
21	54114.5593874(23)	53895.11820(34)	53679.57672240(44)	53810.394847(29)	53579.461957(13)
22	54144.57631255(78)	53895.4042642(11)	53703.50950421(20)	53814.7725655(12)	53602.0488562(37)
23	54169.807929(43)	53920.2922392(15)	53769.86854919(16)	54016.1476506(15)	53625.14909317(57)
24	54202.4350143(10)	53955.1926179(84)	53803.59198568(20)	54074.1524401(18)	53625.66243175(64)
25	54386.88664719(84)	53980.9387988(51)	53804.67983887(39)	54138.7238191(21)	53639.0092353(12)
26	54405.1577859(65)	53981.2248674(25)	53805.76769160(20)	54194.5397633(38)	53660.05611565(62)
27	54465.19152(18)	54010.976010(14)	53811.20695520(65)	54500.9803277(11)	53679.04964135(67)
28	54520.004932(11)	54010.97601(16)	53815.19574799(34)	54556.796287(22)	53703.17655098(73)
29	54574.38333165(93)	54050.7395554(32)	53819.54715879(16)	54625.745400(11)	53769.9105473(44)
30	54632.2419688(18)	54093.6498562(58)	53830.78830373(76)	55058.0451269(12)	53804.8175548(19)
31	54715.3322170(31)	54095.6523369(35)	53896.42208417(51)	55136.8440094(81)	53805.3308931(80)
32	54773.1908713(95)	54098.7990923(55)	53957.34184827(28)	55423.5842712(30)	53805.84423(11)
33	54871.0720237(86)	54099.6572983(38)	54016.08591876(19)	55496.9109732(70)	53811.4909528(27)
34	54957.6424492(38)	54099.657298(14)	54018.62424305(94)	56028.803303(13)	53815.59765935(46)
35	55048.5631694(75)	54148.5750408(15)	54074.46738141(38)	56207.1949872(16)	53819.70436542(79)
36	55625.4094764(43)	54153.438208(24)	54138.65073591(29)	56588.0557186(48)	53829.97113088(95)
37	55664.56195259(61)	54160.5899248(34)	54194.49388733(47)	56745.6533882(18)	53897.2184807(26)
38	55833.7876745(14)	54187.480380(34)	54380.15431237(37)	56778.4862517(19)	53957.27904429(98)
39	55932.5389399(19)	54383.723481(18)	54438.53583792(23)	57026.9214416(40)	54016.31291936(65)
40	56026.5048941(99)	54388.872716(97)	54500.90618449(26)	57118.853363(42)	54017.339595(20)
41	56032.5952797(13)	54390.8751970(34)	54557.11203850(57)	57388.0825864(73)	54074.8334548(22)
42	56298.8320989(10)	54398.8851194(28)	54626.37216650(15)	57770.0376157(17)	54139.00072730(58)
43	56390.62289484(77)	54402.0318746(98)	55057.88815504(46)	57791.9261454(15)	54438.7902578(11)
44	56397.5833346(12)	54404.606492(35)	55136.93909113(38)	58113.6875807(49)	54500.9041975(31)
45	56418.4646542(21)	54406.0368357(75)	55423.04502125(36)	58215.469372(10)	54557.371412(14)

46	56421.5098467(85)	54408.897522(11)	55496.65645520(22)	58320.5344765(64)	54627.18543776(44)
47	56443.2612220(43)	54416.907445(11)	55614.50729843(35)	58385.1057517(27)	55058.389480(10)
48	56471.102983(20)	54419.7681312(71)	55653.30743345(13)	58676.2238832(41)	55137.95685828(45)
49	56479.36850580(72)	54463.5366351(17)	55743.23673378(17)	59037.3857265(58)	55423.3726304(14)
50	56738.6449081(70)	54714.9909962(15)	55829.90249209(13)	59146.828722(66)	55473.16638388(77)
51	56759.5262106(42)	55144.666093(59)	55931.435715350(52)	59317.5597674(69)	55496.7799150(69)
52	56837.39614888(80)	55336.3320909(47)	56023.178350109(53)	59351.4870831(14)	55614.8475620(14)
53	56956.1586525(39)	55489.950956(25)	56028.25501932(28)	59362.4313778(11)	55653.3478840(38)
54	57137.5650962(27)	55625.5474924(31)	56113.107928159(62)	59565.9952139(16)	55744.2086697(10)
55	57172.36728814(36)	55743.979907(30)	56206.663658990(57)	59599.9225153(11)	55829.93609672(77)
56	57186.2881646(17)	55833.805455(24)	56299.49408154(13)	59644.7941078(12)	55931.5769912(83)
57	57187.158219(59)	56026.3296321(39)	56389.42339918(15)	59814.4306563(16)	56023.46444506(70)
58	57261.98292717(47)	56111.2920066(65)	56399.21408991(27)	59947.9510930(19)	56112.78521260(35)
59	57297.2201417(17)	56207.697123(23)	56474.2760313(14)		56299.6402657(27)
60	57333.76243713(41)	56298.3808647(18)	56587.77551551(17)		56389.4744682(18)
61	57382.9205236(13)	56390.494948(27)	56671.54035858(18)		56587.62313967(64)
62	57482.97680593(53)	56397.3605938(19)	56742.25094883(10)		56671.29733409(34)
63	57574.332557(16)	56479.1762070(18)	56745.151897270(95)		56745.2180710(28)
64	58034.5917351(20)	56565.8549853(24)	56778.150170296(93)		56778.07171593(69)
65	58224.263641(60)	56668.5536037(44)	56787.2156265(31)		56838.1322731(19)
66	58313.009213(11)	56738.354336(18)	56837.98220724(13)		56941.8265555(32)
67	58320.8397053(16)	56781.2646226(25)	56941.691102344(90)		56943.8799059(11)
68	58401.7547898(19)	56837.0479954(15)	56943.86681720(26)		57026.527250(36)
69	58937.2735506(36)	56955.7664570(40)	57026.54389180(17)		57119.44131923(56)
70	59029.4994048(23)	56957.7689371(31)	57119.37433252(49)		57209.2754125(11)
71	59156.96251753(89)	57055.6043941(16)	57209.30382670(15)		57299.62286626(52)
72	59255.71383447(71)	57137.133943(18)	57299.595923627(66)		57387.4036938(42)
73	60084.4415596(26)	57224.0987970(19)	57306.12306245(14)		57573.2320873(19)
74		57382.580804(12)	57387.712290037(85)		57769.32723824(31)
75		57480.4162691(17)	57573.01043610(22)		57791.400786(10)
76		57482.4187494(17)	57769.54961759(21)		57875.0749152(29)
77		57571.958225(19)	57791.66932139(23)		58030.6163945(21)
78		57779.357971(28)	57875.07145397(13)		58113.77717324(39)
79		58127.503465(12)	58030.99724588(19)		58305.2522899(10)
80		58224.480718(10)	58113.67431029(38)		58320.1390987(16)
81		58385.8233995(14)	58305.1372071(12)		58412.5399472(14)
82		58386.9676739(16)	58384.9134355(16)		58491.593995(11)
83		58496.8180077(23)	58412.8351305(14)		58582.45486735(75)
84		58582.352511(19)	58582.1782558(12)		58675.8824303(18)
85		58585.4992656(36)	58933.19292746(61)		58753.9098546(79)
86		58586.357471(23)	59020.94654577(18)		58844.7707124(12)
87		58668.17308301(75)	59036.90176275(19)		59020.84561611(69)
88		58754.851860(46)	59076.06457880(74)		59037.27243050(41)
89		58760.859300(72)	59351.29256505(59)		59075.77276022(81)
90		58846.6798719(48)	59565.6005516(11)		59146.6133467(18)
91		58937.3636098(19)	59599.68674527(20)		59246.71413578(97)
92		59029.1916226(28)	59644.28887715(32)		59317.5547223(18)
93		59264.3399930(18)	59705.2088602(36)		59351.43499999(36)
94		59325.5586680(37)	59947.43818330(32)		59362.2150910(84)
95		59325.5586680(24)	60110.97913770(26)		59565.4968589(40)

96	59454.003456(10)	59599.3771697(16)
97	59604.76158787(98)	59644.55092666(54)
98	59640.5201577(16)	59705.124824(25)
99	59700.308487(29)	59813.9523949(92)
100	59893.976925(16)	59947.4203255(39)

Table 2. Timing Parameters for the Ter5 RBs.

Parameter	Ter5P	Ter5ad	Ter5ar
Pulsar Name	PSR J1748–2446P	PSR J1748–2446ad	PSR J1748–2446ar
Data Reduction			
Span of Timing Data (MJD)	53204–60111	53320–59948	53193–59948
Number of TOAs	1536	388	495
RMS TOA Residual (μ s)	40.7	31.4	66.5
Reduced χ^2	1.01	1.03	1.02
EFAC for incoherent data	2.52	2.65	3.47
EFAC for coherent data	5.79	4.07	4.86
Timing Parameters			
Right Ascension (RA, J2000)	17 ^h 48 ^m 05 ^s 03815(7)	17 ^h 48 ^m 03 ^s 8479(1)	17 ^h 48 ^m 04 ^s 6196(2)
Declination (DEC, J2000)	–24° 46′ 41″29(3)	–24° 46′ 41″84(5)	–24° 46′ 45″87(8)
Proper Motion in RA (mas yr ^{–1}) ...	–1.8(1)	–2.2(2)	0.3(3)
Pulsar Spin Period (ms)	1.72861982757976(9)	1.3959548139683(1)	1.9528106824465(3)
Pulsar Spin Frequency (Hz)	578.49619913252(3)	716.35556537627(6)	512.08240972300(8)
Spin Frequency Derivative (Hz s ^{–1})	–8.66271(8) $\times 10^{-14}$	1.74117(6) $\times 10^{-14}$	6.76849(7) $\times 10^{-14}$
Frequency 2nd Derivative (Hz s ^{–2})	4(2) $\times 10^{-26}$	–4(2) $\times 10^{-27}$	–1.82(3) $\times 10^{-25}$
Frequency 3rd Derivative (Hz s ^{–3}) .	–2.5(2) $\times 10^{-33}$	–	–
Frequency 4th Derivative (Hz s ^{–4}) .	–4.3(1) $\times 10^{-41}$	–	–
Reference Epoch (PEPOCH, MJD) .	56657.660271337430459	56633.74460856008227	56570.518685778268264
Dispersion Measure (DM, pc cm ^{–3})	238.71(1)	235.63(2)	238.66(1)
DM Derivative (pc cm ^{–3} yr ^{–1})	–0.007(1)	–0.009(2)	–0.001(1)
Orbital Parameters			
Orbital Period (days)	0.362618545(8)	1.09442881(5)	0.513338066(9)
Orbital Period Derivative	1.38(8) $\times 10^{-10}$	0.0(0)	0.0(0)
Projected Semi-Major Axis (lt-s) ...	1.271836(1)	1.102814(3)	1.498546(4)
Ref. Epoch of Periastron (T_0 , MJD)	53800.32842747(6)	53318.995701960084(6)	53495.2744166(2)
Derived Parameters			
Mass Function (M_\odot)	0.01679872(5)	0.001202305(9)	0.0137115(1)
Min Companion Mass (M_\odot)	≥ 0.38	≥ 0.14	≥ 0.35

NOTE—Numbers in parentheses represent 1- σ uncertainties in the last digit as determined by TEMPO, PINT, or via standard error propagation. The timing solutions used the DE440 Solar System Ephemeris and times are all in Barycentric Dynamical Time (TDB), referenced to TT(BIPM2021). The eccentricity and longitude of periastron, ω , for each of the binaries were each assumed to be zero. Minimum companion masses were calculated assuming a pulsar mass of $1.4 M_\odot$.

Table 3. Timing Parameters for M28H and NGC 6440D.

Parameter	M28H	NGC6440D
Pulsar Name	PSR J1824–2452H	PSR J1748–2021D
Data Reduction		
Span of Timing Data (MJD)	53629–60084	53478–59894
Number of TOAs	866	574
RMS TOA Residual (μ s)	46.1	31.9
Reduced χ^2	1.01	1.02
EFAC for incoherent data	2.75	1.47
EFAC for coherent data	7.37	1.32
Timing Parameters		
Right Ascension (RA, J2000)	18 ^h 24 ^m 31 ^s 6098(2)	17 ^h 48 ^m 51 ^s 6457(1)
Declination (DEC, J2000)	–24° 52′ 17″15(4)	–20° 21′ 07″41(2)
Proper Motion in RA (mas yr ^{–1}) ...	–1.1(3)	–1.4(2)
Pulsar Spin Period (ms)	4.6294137643019(6)	13.4958205400413(8)
Pulsar Spin Frequency (Hz)	216.01007188235(3)	74.097013740888(5)
Spin Frequency Derivative (Hz s ^{–1})	–3.6139(2) × 10 ^{–15}	–3.22033(1) × 10 ^{–15}
Frequency 2nd Derivative (Hz s ^{–2})	–8(9) × 10 ^{–28}	5(2) × 10 ^{–28}
Reference Epoch (PEPOCH, MJD) .	56856.714649097440997	56686.128079588925175
Dispersion Measure (DM, pc cm ^{–3})	121.38(2)	224.999(6)
DM Derivative (pc cm ^{–3} yr ^{–1})	0.014(3)	–0.004(1)
Orbital Parameters		
Orbital Period (days)	0.43502746(1)	0.2860686141(6)
Orbital Period Derivative	0.0(0)	–1.7(1) × 10 ^{–11}
Projected Semi-Major Axis (lt-s) ...	0.719473(4)	0.397212(1)
Ref. Epoch of Periastron (T_0 , MJD)	53755.2263970(4)	56479.176207(1)
Derived Parameters		
Mass Function (M_\odot)	0.00211297(3)	0.000822259(9)
Min Companion Mass (M_\odot)	≥ 0.17	≥ 0.12

NOTE—Numbers in parentheses represent 1- σ uncertainties in the last digit as determined by TEMPO, PINT, or via standard error propagation. The timing solutions used the DE440 Solar System Ephemeris and times are all in Barycentric Dynamical Time (TDB), referenced to TT(BIPM2021). The eccentricity and longitude of periastron, ω , for each of the binaries were each assumed to be zero. Minimum companion masses were calculated assuming a pulsar mass of 1.4 M_\odot .